9-2016

Nucleon Decay, Atmospheric Neutrinos, and Cosmic Rays at DUNE: September 2016 Progress Report

E. Church
Northwest National Laboratory,

D. Dwyer
Lawrence Berkeley National Laboratory,

H. Gallagher
Tufts University

M. Goodman
Argonne National Laboratory

R. Hatcher
Fermi National Accelerator Laboratory

See next page for additional authors

Authors
E. Church, D. Dwyer, H. Gallagher, M. Goodman, R. Hatcher, J. Hewes, A. Higuera, V. A. Kudryavtsev, L. Lin, N. Martinez, H. Méndez, J. L. Raaf, M. Robinson, G. Santucci, M. Sorel, A. Tonazzo, T. K. Warburton, K. Wood, and T. Yang

Nucleon Decay, Atmospheric Neutrinos, and Cosmic Rays at DUNE: September 2016 Progress Report

E. Church,[1] D. Dwyer,[2] H. Gallagher,[3] M. Goodman,[4] R. Hatcher,[5] J. Hewes,[6] A. Higuera,[7] V. A. Kudryavtsev,[8] L. Lin,[4] N. Martinez,[9] H. Méndez,[9] J. L. Raaf,[5] M. Robinson,[8] G. Santucci,[10] M. Sorel,[11] A. Tonazzo,[12] T. K. Warburton,[8] K. Wood,[10] and T. Yang[5]

[1]*Pacific Northwest National Laboratory, Richland, Washington, USA*

[2]*Lawrence Berkeley National Laboratory, Berkeley CA, USA*

[3]*Department of Physics and Astronomy, Tufts University, Medford, MA, USA*

[4]*Argonne National Laboratory, Lemont, IL, USA*

[5]*Fermi National Accelerator Laboratory, Batavia IL, USA*

[6]*School of Physics and Astronomy, University of Manchester, Manchester, UK*

[7]*Department of Physics, University of Houston, Houston, TX, USA*

[8]*Department of Physics and Astronomy, University of Sheffield, Sheffield S3 7RH, UK*

[9]*Departamento di Física, Universidad de Puerto Rico en Mayagüez, Mayagüez, Puerto Rico*

[10]*Department of Physics and Astronomy, Stony Brook University, Stony Brook, NY, USA*

[11]*Instituto de Fisica Corpuscular, Valencia, Spain*

[12]*APC Laboratory, Université Paris-Diderot, Paris, France*

I. INTRODUCTION

We report on the progress made within the Nucleon Decay, Atmospheric Neutrinos, and Cosmogenics Physics Working Groups since the DUNE CDR, and in particular in the period September 2015 – September 2016. This note is also intended to provide input for the September 2016 Preliminary Report of the Far Detector Task Force. We report jointly for the three WGs since they are tightly coupled. They make use of the same DUNE Far Detector for their physics studies, they share the same energy regime, and they are all characterized by random, non-beam triggers. Finally, cosmogenic events are a background for atmospheric neutrino physics, and both cosmogenic events and atmospheric neutrinos are a background for nucleon decay physics. Recent progress within the Nucleon Decay, Atmospheric Neutrinos and Cosmogenics Physics Working Groups is reported in Secs. II, III and IV, respectively.

II. NUCLEON DECAY PHYSICS

The purpose of the DUNE Nucleon Decay (NDK) Physics WG is to evaluate and demonstrate the experimental sensitivity of DUNE to various nucleon decay modes and other baryon number non-conserving processes, such as neutron-antineutron oscillations. Sensitivity to a specific NDK mode is expressed in terms of the partial lifetime τ/B, where B is the branching fraction of the NDK mode being considered. Experimentally, the τ/B sensitivity can be written as:

$$\tau/B = n \cdot \varepsilon \cdot Mt/N_S \tag{1}$$

where n is the number of protons or neutrons (depending on the NDK mode) per unit mass, ε is the signal selection efficiency, Mt is the detector exposure, N_S is the largest number of signal events compatible with a background-only data sample. The lower the background rate, the lower N_S, and hence the higher the τ/B sensitivity. DUNE sensitivities reported in the CDR [1] for the $p \to \bar{\nu}K^+$ mode, as well as in earlier studies, assumed preliminary estimates for the signal efficiency and background rates [2]. An important goal of the NDK Physics WG, and of this Far Detector Task Force, is to refine these estimates via fully simulated and reconstructed event samples. Another important goal is to extend DUNE NDK studies to promising modes other than $p \to \bar{\nu}K^+$. This Section focuses on

recent progress toward full simulation, reconstruction, and analysis for NDK signal events. The focus will be on $p \to \bar{\nu}K^+$, but other modes will be discussed as well. Cosmogenic backgrounds to NDK are discussed in Sec. IV.

The simulation of NDK events includes the NDK event generation within GENIE [3, 4], the tracking of particles through the DUNE far detector geometry within Geant4, and the hit-level simulation through LArSoft's detsim module. The last two steps are common to other physics measurements and searches, and are discussed elsewhere. We focus here on NDK event generation.

GENIE is used for generation of nucleon decay events, since the treatment of nuclear effects on the initial and final nuclear state are common with the modeling of neutrino interactions, GENIE's primary physics goal. During the last year, we have made major progress both within GENIE, and concerning GENIE-LArSoft integration for NDK simulation. A summary of the GENIE and LArSoft-related tasks accomplished by the NDK working group is listed here:

1. **Upgraded GENIE to include the full 68 exclusive nucleon decay modes listed by the Particle Data Group**

   The current GENIE production release (v2.10) can only simulate 11 NDK modes, which are all $(B - L)$-conserving antilepton plus meson modes, see [3, 4]. However, the Particle Data Group reports experimental searches for as many as 68 exclusive modes [5]. These modes include 2, 3, or 5 particles in the final state. They include antilepton plus meson(s), lepton plus meson(s), antilepton plus photon(s), and three (or more) leptons decay modes. A GENIE Incubator Project to upgrade GENIE to include all such NDK channels has been created [6]. The code exists in a GENIE development branch and is under review by the GENIE team. The goal is to include this upgrade in the GENIE v2.12 production release.

2. **Improved the GENIE-LArSoft interface to allow seamless event generation without the awkward step that was previously required to bridge the two formerly-independent pieces of software via an ASCII file**

   Until recently, NDK event generation consisted of a LArSoft module reading GENIE event records in ASCII format, assigning decay vertices with the argon of the detector geometry being used. This approach had the disadvantage that it required running

a stand-alone GENIE application. We are now able to simulate GENIE NDK events directly within the LArSoft module, through calls to the appropriate GENIE libraries, hence avoiding the need of a separate GENIE executable [7]. This greatly simplifies the production of NDK event samples as part of DUNE official Monte-Carlo productions.

3. **Identified and fixed a bug in GENIE related to kaon inelastic interactions**
   In GENIE (v2.10), kaon inelastic interactions have no particles in the final state for NDK-generated kaons, as in $p \to \bar{\nu}K^+$. This has now been fixed, resulting in only 0.2% of K^+ being lost within the Ar nucleus in $p \to \bar{\nu}K^+$ events, according to GENIE [8]. This is to be compared with the 3.2% number in Ref. [2], based on the FLUKA [9] modeling of $K^+ + n \to K^0 + p$ charge-exchange reactions within the Ar nucleus.

4. **Identified and fixed a bug in LArSoft in which NDK event vertices were incorrectly distributed through the argon volume**
   In LArSoft, NDK vertices were incorrectly assumed to follow a gaussian distribution within the Ar volume. This has now been changed to follow a uniform distribution [10]. Examples of fully simulated NDK events within the DUNE 1×2×6 far detector geometry are shown in Figs. 1 and 2. Fig. 1 shows a $p \to \mu^+ K^0$ event, a promising mode whose study in DUNE has been enabled by the recent simulation upgrades. Fig. 2 shows a $p \to \bar{\nu}K^+$ "golden" mode event.

5. **Upgraded GENIE to simulate neutron-antineutron oscillation**
   A GENIE Incubator Project for neutron-antineutron oscillation simulation has been created [11]. This module is under review by the GENIE collaboration, and will also be included in a future GENIE production release.

Progress has also been made in validating and improving reconstruction for NDK events. In addition to high tracking efficiency, excellent particle identification though the measurement of the dE/dx profile of stopping particles is crucial for NDK physics. DUNE aims not only to efficiently reconstruct, but also to identify, all charged particles produced in NDK events. The NDK working group has made progress in the following topics related to event reconstruction and particle identification:

1. **Evaluating tracking efficiencies for particles produced in $p \to \bar{\nu}K^+$ events, using the Projection Matching Algorithm (PMA, [14])**

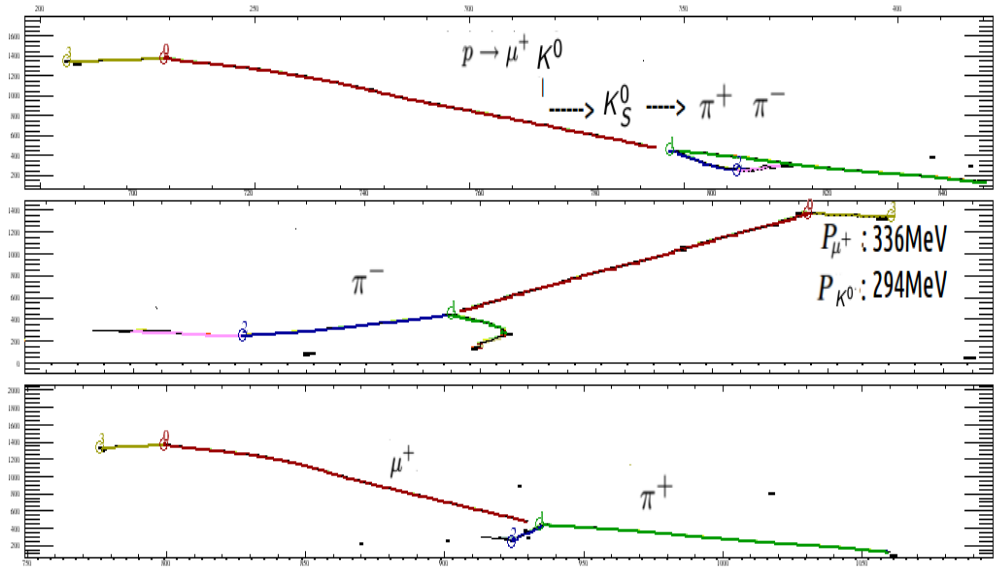

FIG. 1. Event display of a simulated $p \to \mu^+ K^0$ event in DUNE, where $\mu^+ \to e^+ \nu_e \bar{\nu}_\mu$ and $K^0_S \to \pi^+ \pi^-$. From [12].

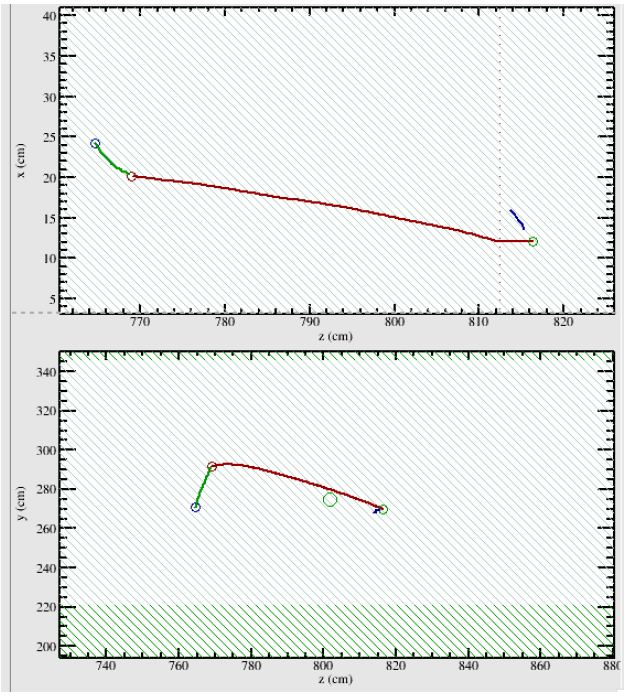

FIG. 2. Event display of a simulated $p \to \bar{\nu} K^+$ event in DUNE, where $K^+ \to \mu^+ \nu_\mu$ and $\mu^+ \to e^+ \nu_e \bar{\nu}_\mu$. The green track is the reconstructed kaon track, the red is the muon, and blue is the positron. From [13].

For K^+'s, the default PMA algorithm used for long-baseline oscillation physics studies results in a 64% overall tracking efficiency for K^+'s [15]. The efficiency is highly momentum-dependent, with an efficiency exceeding 80% for > 0.3 GeV/c kaons, as shown in the left panel of Fig. 3. In $p \to \bar{\nu} K^+$ events, kaons are expected to have momenta distributed in the 0.1–0.5 GeV/c range, because although the decay produces a monoenergetic kaon, its momentum can be modified by Fermi momentum as the kaon escapes the nucleus. The efficiency for μ^+ and e^+ produced in $K^+ \to \mu^+ \nu_\mu$ decays (63.6% branching fraction) is not shown here, but is somewhat higher. We expect that improvements can be made during the next months by customizing the reconstruction algorithms for better performance to relatively low momenta ($\sim$0.1 GeV/c). As an example, the left panel of Fig. 3 shows the results for K^+ tracking efficiency using an alternative cluster algorithm (TrajCluster module) compared to the standard algorithm for tracks (LineCluster module). Tracking performance is also being evaluated in terms of single-track momentum and direction resolution, and for invariant mass resolution for two-body decays of neutral mesons (π^0, K^0_S, ρ^0) [12, 15].

2. **Evaluating PID efficiencies and mis-ID rates for $e/\mu/\pi/K/p$ separation [12, 13]**

   Distributions from a particle identification algorithm (PIDA, [16]) applied to all reconstructed particles in simulated $p \to \bar{\nu} K^+$ events is shown in the right panel of Fig. 3. The algorithm is applied here only on the last 15 cm of the tracks. Studies are in progress to understand the current status and improve where possible. An important difference between beam and NDK events is that no preferred direction exists in the latter case, and detector-only information can be used to determine the track direction. We have verified with ($p \to \bar{\nu} K^+$, $K^+ \to \mu^+ \nu_\mu$) events that the same dE/dx information along the track works very well also to determine the K^+ track direction, and hence the NDK vertex [13].

3. **Assessing photon detector performance in relation to NDK physics [17]**

   The photon detector system (PDS) is sensitive to the primary scintillation light from Ar de-excitation and electron-ion recombination. The PDS is particularly important to enable non-beam physics discussed here, especially to provide drift position determination and hence fiducial volume definition. About 10^3 photo-electrons (PEs) are

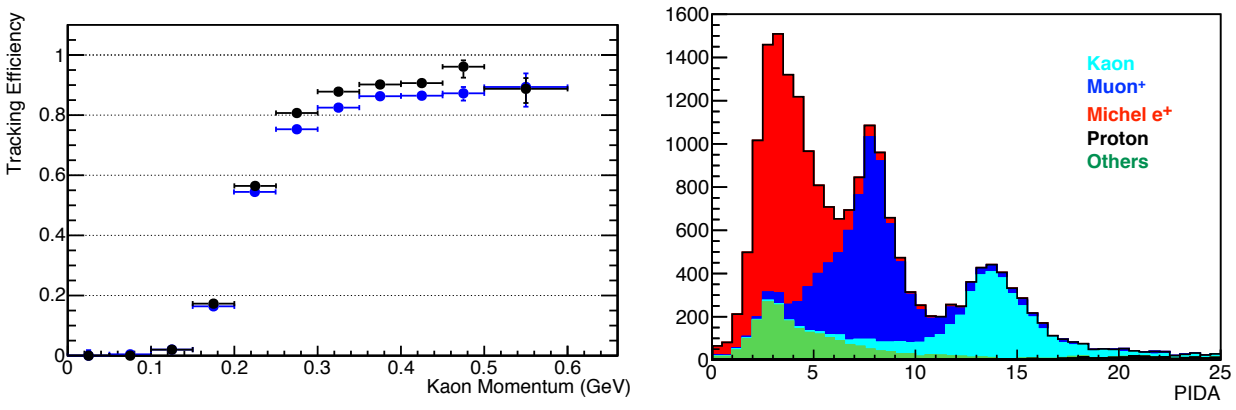

FIG. 3. Left panel: K^+ tracking efficiency versus K^+ momentum in $p \to \bar{\nu}K^+$ events. Blue symbols: using standard 2D clustering algorithm (LineCluster) as tracking input. Black symbols: using alternative clustering (TrajCluster). Right panel: PIDA distribution for reconstructed particles in $p \to \bar{\nu}K^+$ events where $K^+ \to \mu^+\nu_\mu$. PIDA is computed using the last 15 cm of the tracks. From [13].

expected on average for $p \to \bar{\nu}K^+$ events and the current PDS assumptions. The amount of detected light varies greatly with the distance between the NDK vertex and the APA plane where the PDS is installed. Figure 4 shows the efficiency to reconstruct a flash of light as a function of such distance, and for different PE thresholds for the PDS (in the 2–20 PE range). The efficiency is satisfactory: it is greater than 97% for NDK vertex-APA distances lower than 340 cm. Fake associations between charge and light signals might be produced by light flashes from ^{39}Ar radioactive decays. The number of reconstructed ^{39}Ar flashes can be significant for few-PEs thresholds, as also shown in Fig. 4. In the future, the spatial reconstruction of the flash across several PDS elements will be studied to discriminate flashes of light between ^{39}Ar, NDK, atmospheric neutrino and cosmogenic events.

As far as NDK analysis, the focus has been on:

1. **Identification of promising NDK modes**

   A comprehensive list of NDK modes where DUNE may have an early discovery potential has been produced [18], see Tab. I. In this context, early discovery potential is defined as DUNE having a sensitivity after a 40 kton·yr exposure that is potentially greater than the current limit and the Super-Kamiokande sensitivity extrapolated to

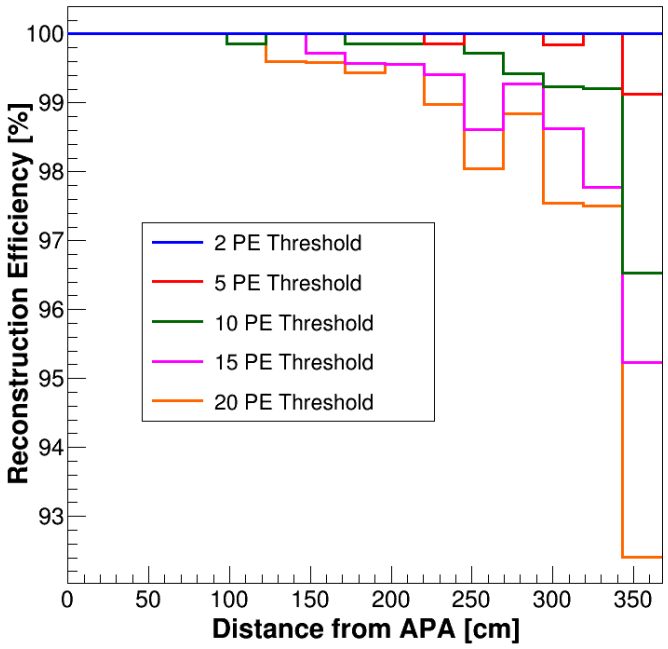

Threshold (PEs)	^{39}Ar flashes (#/APA/drift)
2	30
5	3
10	0.08
15	0.004
20	0.0003

FIG. 4. Flash finding efficiency for $p \to \bar{\nu} K^+$ events, as a function of the flash distance from the clostest APA and for different PE thresholds. The table at the right indicates the expected rate of ^{39}Ar flashes above threshold. From [17].

the year 2025. The assumed DUNE sensitivities account for nuclear effects responsible for irreducible efficiency losses. However, they should be regarded as rough indications only, as they assume zero background and approximate reconstruction efficiencies. Nonetheless, they provide a useful subset of modes that are candidates for more realistic Monte-Carlo simulations. As the table shows, DUNE is expected to do well in NDK modes with charged or neutral kaons in the final state, or in multi-prong decays. Modes with neutrinos in the final state may also be promising. They are, however, not listed in Tab. I, as reliable estimates for their relatively large backgrounds are particularly important in this case.

2. **Evaluating NDK signal efficiencies**

   A realistic estimate of NDK signal efficiencies for fully reconstructed $p \to \bar{\nu} K^+$, $p \to l^+ \rho^0$ and $p \to \mu^+ K^0$ events has just started [12, 13], and will continue to make progress in coming months.

3. **Evaluating NDK background rates**

   A realistic estimate of NDK backgrounds from both cosmogenically-induced events

TABLE I. List of possible NDK modes where DUNE may have an early discovery potential. See text for details. The current limits for these modes are also shown in the table. Adapted from [18].

Mode	PDG ID	Current Limit (10^{33} yr)
$n \to e^+ K^-$	13	> 0.017
$p \to e^+ K^0$	13	> 1.0
$n \to \mu^+ K^-$	16	> 0.026
$p \to \mu^+ K^0$	16	> 1.6
$p \to e^+ K^{*0}$	21	> 0.084
$n \to e^- K^+$	34	> 0.032
$n \to \mu^- K^+$	35	> 0.057
$p \to e^- \pi^+ K^+$	40	> 0.075
$p \to \mu^- \pi^+ K^+$	41	> 0.245

and from atmospheric neutrino events is a critical component of these analyses. Cosmogenic background studies are discussed in more detail Section IV. Studies of atmospheric neutrino backgrounds are just beginning.

4. **Evaluating NDK sensitivities**

   Python-based scripts have been developed to evaluate DUNE sensitivities as a function of exposure, signal efficiency, and background rate assumptions. These are available to the collaboration [19].

The NDK working group has made good progress over the last year in each of the areas that is critical for the success of NDK searches in DUNE. Although there is still much work to be done, the forward motion over the past year is largely thanks to the efforts of our dedicated working group members.

III. ATMOSPHERIC NEUTRINO PHYSICS

Atmospheric neutrino studies for LBNE and LAGUNA-LBNO relied on smeared truth-level quantities rather than full simulations and reconstruction. These previous studies focused on the neutrino mass hierarchy, determining the octant of θ_{23}, and observation of CP violation. In DUNE the focus of effort has been to continue the study of interesting physics

signatures, and to move away from truth-level studies to full simulation and reconstruction.

Atmospheric Neutrino Simulation and Reconstruction: Within LArSoft, users can now generate and process atmospheric neutrino events through all of the necessary stages: event generation with GENIE, GEANT simulation of energy deposition, detector simulation, reconstruction, and analysis. The current LArSoft configurations allow one to simulate events using the Bartol atmospheric neutrino fluxes calculated at solar max or solar min [20]. Improvements have been made to numerous elements of this software stack, and areas where further work is necessary have been identified.

The generation stage brings together the detector mass model, an atmospheric neutrino flux calculation, and the neutrino interaction cross sections, using a piece of GENIE code known as the Event Generation Driver. Several groups world-wide carry out calculations of atmospheric neutrino fluxes [20–22], and the GENIE flux drivers have been extended so that they are able to use calculations from all of these groups. Most of these groups have now performed calculations for the geomagnetic location of the Homestake site, and we hope in the future to also have calculations which include the local topography [23]. The addition of the ATMNC flux [22] necessitated changes to the structure of the GENIE atmospheric event drivers, as this computation included additional information, such as the azimuthal-angle dependence of the flux, and direction-dependent production height tables, which were not included in previous flux calculations. Some additional work will be required to extend the GENIE output record in order to pass through needed flux-related information, such as the neutrino production height, for the purposes of downstream analyses. The existing drivers are rather slow - arising from the fact that atmospheric neutrinos have a broad and rapidly falling energy spectrum, and by default GENIE strobes neutrinos through the full detector in order to compute the probability of interaction (relative to the maximum probability which it also determines). This has not proved to be a bottleneck for analyses studies to date, but is an area where significant speedup is possible.

There has also been improvement on the cross section side of GENIE with the incorporation of the Athar et al. model for neutrino $\Delta S = 1$ scattering into GENIE release 2.10.0 [24, 25]. This model, which provides an improved description of $\Delta S = 1$ CC interactions up to 3 GeV, is not turned on by default, but is expected to be part of a comprehensively retuned version of GENIE available in the future.

Atmospheric neutrino interactions have been carried through the entire simulation and

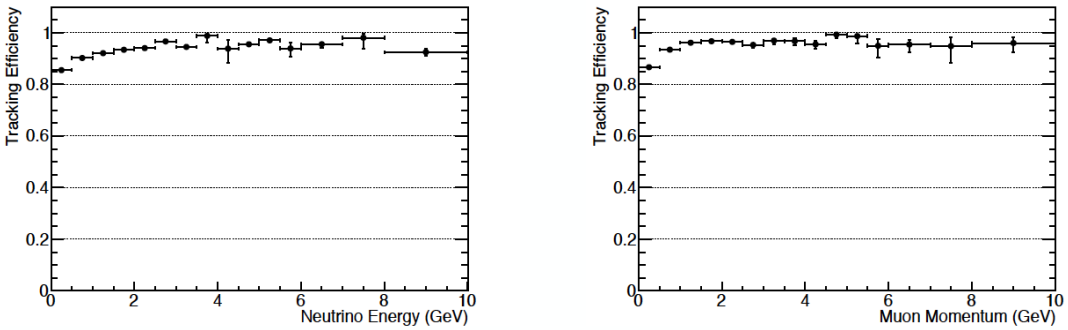

FIG. 5. Muon tracking efficiency for atmospheric muon neutrino CC interactions as a function of neutrino energy (left) and muon momentum (right). From [15].

analysis framework, and preliminary studies on how well the reconstruction works on these events have been performed [15]. Figure 5 shows the muon tracking efficiency for atmospheric muon neutrino CC interactions as a function of neutrino energy and muon momentum. Overall the muon tracking performance is found to be similar to that for beam neutrinos, with tracking failures most often occurring when muons are traveling parallel to the electron drift. As the atmospheric neutrino beam is arriving from all directions this particularly challenging orientation can be achieved for any muon (or neutrino) energy. Understanding the energy and angular dependence of these efficiency curves will be important for atmospheric neutrino studies which rely on resolving features of neutrino oscillograms.

The previous studies demonstrated that DUNEs excellent neutrino energy and pointing resolution can compensate for the relatively small fiducial volume, resulting in competitive physics sensitivities. The mass hierarchy sensitivity, for instance, relies primarily on measurement of neutrinos with energies from 1 to 10 GeV, an energy regime largely insensitive to some of the detector optimization decisions currently being debated. Over the past year we have therefore tried to encourage study of additional DUNE physics topics that might take advantage of these same strengths for lower energy interactions. Two examples are the study of matter effects using low energy atmospheric neutrinos [26], and the measurement of the neutrino azimuthal energy dependence [27]. The measurement of the azimuthal dependence of atmospheric neutrinos has been carried out by the SuperKamiokande experiment [28], and a comparable measurement by DUNE could potentially be done with a significantly smaller data set and serve as a valuable early demonstration that the detector is capable

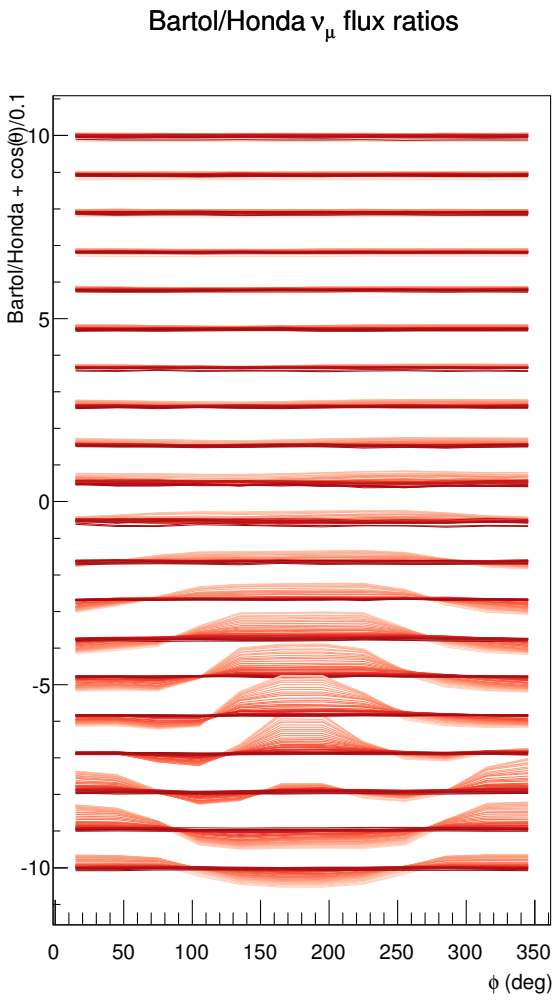

FIG. 6. Ratio of the Honda to Bartol flux calculation for muon neutrinos. Each band corresponds to the flux in a zenith angle bin of $\cos(\theta) = 0.1$, with downgoing neutrinos in the top band. Within each band are ten colored lines corresponding to increasing neutrino energies in 1 GeV bins from 0 to 10 GeV. From [27].

of achieving high resolution measurements. This validation would be particularly important as more data is acquired and we attempt to discern other features from the measured flavor-energy-angle dependent oscillograms. For a particular bin of zenith angle, flavor, and energy, neutrino oscillation probabilities are independent of neutrino azimuthal angle, and flux calculations predict significant non-isotropies resulting from the geomagnetic shielding of low energy primaries. Figure 6 shows the ratio of Honda and Bartol flux predictions for muon neutrinos, as a function of zenith angle, azimuthal angle, and energy.

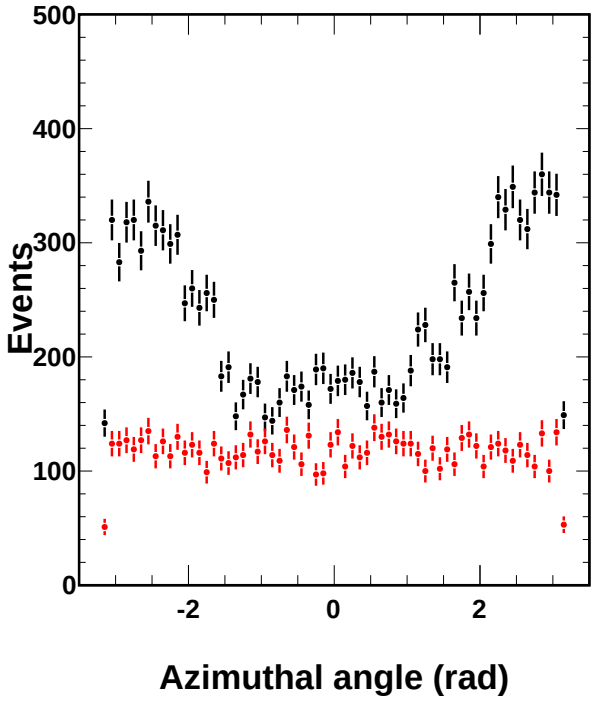

FIG. 7. True azimuthal angle distribution for atmospheric neutrino interactions with $\cos(\theta) < -0.7$, from a sample of 500k simulated atmospheric neutrino interactions [29]. $E_\nu < 0.5$ GeV (black) and $E_\nu > 3$ GeV (red).

In this calculation, the flux driver used for the Bartol flux did not include azimuthal information, so the flux was taken to be isotropic in azimuthal angle. The plot demonstrates several features the East/West asymmetry for incoming neutrinos, and the relatively large fluxes of low energy neutrinos arriving from the Earths polar regions (as seen from a detector at the Homestake site).

This results from the fact that the magnetic shielding of the Earth is smallest at the poles. Figure 7 shows the true azimuthal angle distribution for atmospheric neutrino interactions with $\cos(\theta) < -0.7$, a region covering the South pole, from a sample of 500k simulated atmospheric neutrino interactions. The black points correspond to events with $E_\nu < 0.5$ GeV, red to $E_\nu > 3$ GeV, clearly showing the large variation for low energy neutrinos. Figure 8 shows the expected DUNE azimuthal angle resolution for $E_\nu < 1$ GeV interactions, which is clearly sufficient for resolving these expected features in the atmospheric flux.

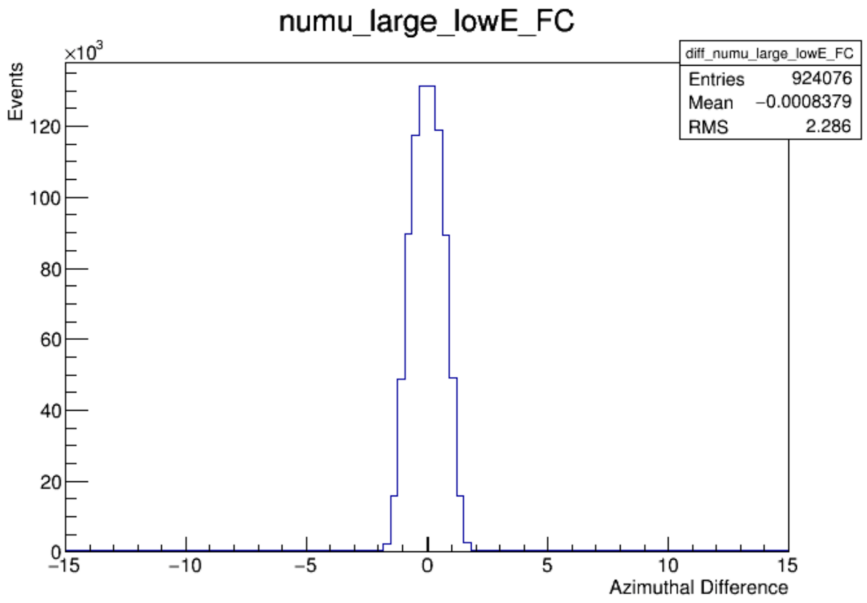

FIG. 8. Azimuthal angle resolution for ν_μ CC interactions with $E_\nu < 1$ GeV [27].

IV. COSMIC RAYS AND COSMOGENICS

A. Muon generator: MUSUN

The muon generator for the DUNE far detector (FD) is based on the well-known muon simulation code MUSUN (MUon Simulations UNderground) [30, 31]. The code uses the results of muon transport through rock carried out with the MUSIC code [30, 32, 33] convolved with the muon spectrum at sea level for different zenith angles. The MUSUN code, originally written as a standalone package in FORTRAN, has been converted into a module in LArSoft (written in C++) and tested with respect to the original code.

The MUSUN code, as currently adapted for DUNE, samples muons around an underground laboratory located near the Ross shaft and expected to host one of the 10 kt modules of the future DUNE experiment. The global coordinates of the location: latitude = 44°20′45.21” N, longitude = 103°45′16.13” W. The rock composition has been taken from Refs. [34, 35]. Many rock samples have been measured and the average rock composition has been calculated as $< Z >= 12.09$ and $< A >= 24.17$ [34, 35]. The average density of rock was assumed to be 2.70 g/cm^3 [35] in the MUSIC simulation for SURF. Other measurements suggest that the density may be larger (2.8-2.9 g/cm^3 [36, 37]). The density can be changed in the MUSUN muon generator if required. The slant depth distribution for the

4850 ft level at SURF was calculated from the CGIAR digital elevation model [38].

The measurement of the muon flux at SURF (in the Davis' campus near the Yates shaft) was performed by the active veto system of the Davis' experiment [39] giving the value of $(5.38\pm0.07)\times10^{-9}$ cm^{-2}s^{-1}sr^{-1} for the vertical flux (the measured fraction of multiple muons has been added to the single muon flux as given in Ref. [39], so the systematic uncertainty for this value may be of the order of a few %). The result agrees very well with the vertical flux calculated by MUSIC/MUSUN (in this case the coordinates for the Davis' campus were used to calculate the slant depth distribution for MUSUN): 5.18×10^{-9} cm^{-2}s^{-1}sr^{-1}. A recent measurement of muons in the Davis' campus has been carried out with the active veto system of the Majorana demonstrator [40] giving the value of $(5.04 \pm 0.16) \times 10^{-9}$ cm^{-2}s^{-1} for the total (not vertical) muon flux, in reasonable agreement with a calculation with MUSIC/MUSUN for a close location (also in Davis campus but LUX/LZ location rather than Majorana demonstrator hall): 6.16×10^{-9} cm^{-2}s^{-1}. Given a small difference between the recent measurement and simulations (that can be due to different locations) we estimate the systematic uncertainty in calculating the muon flux in our model as 20%. We emphasize the need for an accurate measurement of the muon flux in the DUNE cavern(s) to normalize simulations.

Figure 9 (left) shows the profile of the surface above the proposed location of the far detector (center of the map). The lines drawn from the center divide each quadrant into 4 angles of equal size, 22.5°, to guide the eye. Muon azimuth angle distribution is plotted in Figure 9 (right). The vertical lines show approximately the division of quadrants on the left figure where the azimuth angle is calculated from East (pointing to the right on the left figure). Moving from East to North and further on counterclockwise on the map on the left, one can see how the dips and peaks on the surface profile correspond to peaks and dips in the number of muons on the graph on the right.

The parameters of the muon flux are given in Table II for simulations carried out with MUSIC/MUSUN. These particular simulations did not include the cavern geometry and assumed spherical geometry for an imaginary detector.

The normalization of the muon flux or rate is done for a specific point underground where the slant depth distribution was calculated. This implies that the cavern/laboratory is relatively small and the muon flux is the same everywhere across the cavern (plus the rock where the box for muon sampling is extended to). For the cavern(s) where the far detector

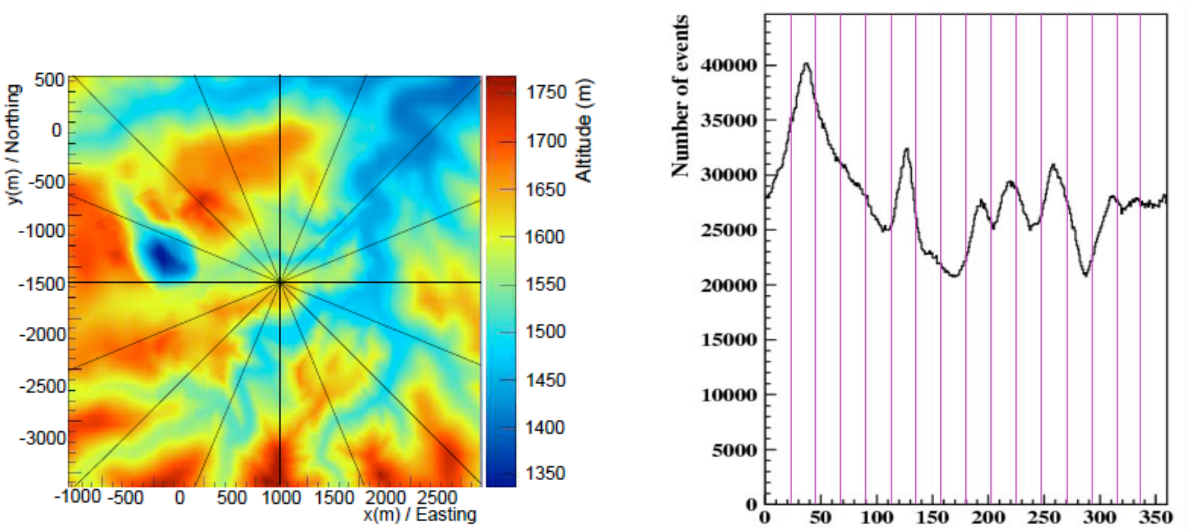

FIG. 9. Left – surface profile above the proposed location for the far detector (center of the map). The lines drawn from the center divide each quadrant into 4 angles equal in size: 22.5° to guide the eye. Right – muon azimuth angle distribution. The vertical lines show the division of quadrants on the left figure where the azimuth angle is calculated from East (pointing to the right on the left figure). Moving from East to North and further on counterclockwise on the map on the left, you can see how the dips and peaks on the surface profile correspond to peaks and dips in the number of muons on the graph on the right.

TABLE II. Muon flux parameters as calculated with MUSIC/MUSUN.

Total flux, $\mathrm{cm}^{-2}\mathrm{s}^{-1}$	Mean E_μ, GeV	Mean slant depth, m w. e.	Mean θ, deg.
5.66×10^{-9}	283	4532	26

will be located the difference in muon intensities in different locations does not exceed 10%.

In the MUSUN generator for DUNE muons are sampled on a surface of a box that encompasses the lab and a few meters of rock around the cavern. The rock is included to make sure that muon-induced cascades initiated above and around the cavern, have enough of space to fully develop and produce, in simulations, potentially dangerous secondaries, whereas the muon itself may not cross the active volume of argon. The size of the box is $74.43 \times 29.54 \times 30.18$ m^3 (length×width×height). The size of the cryostat has been assumed to be $61.62 \times 14.94 \times 13.58$ m^3 (length×width×height). Muons are sampled according to their

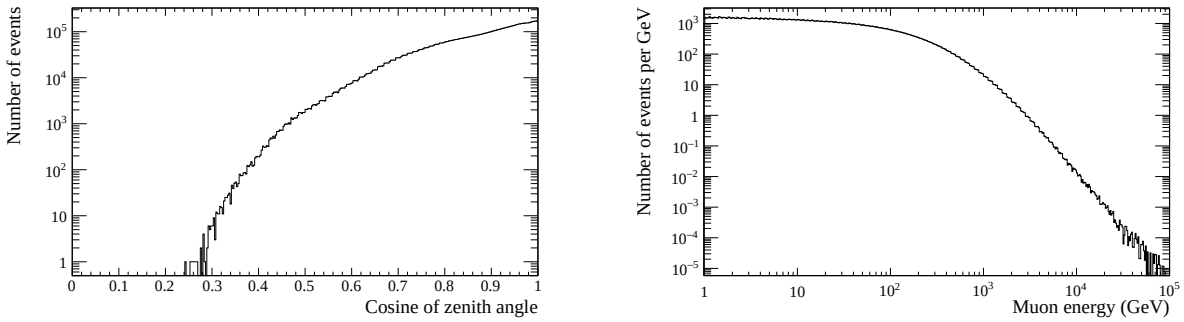

FIG. 10. Left – zenith angle distribution of muons as simulated with the MUSUN muon generator for DUNE, right – energy spectrum of muons at the DUNE site.

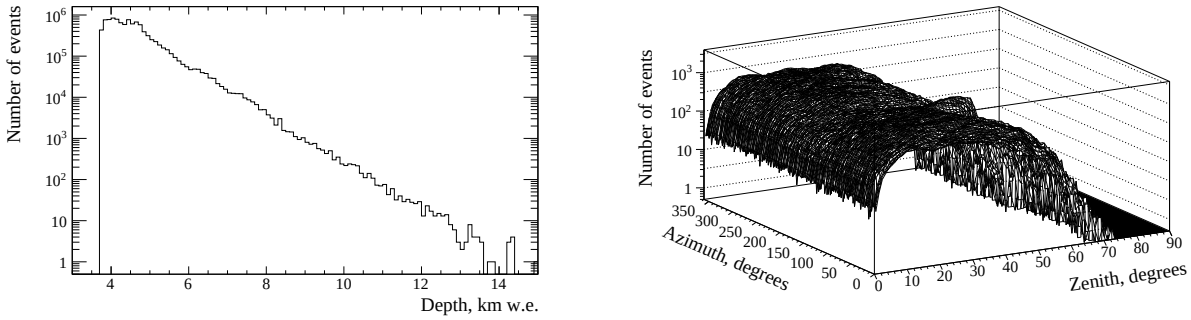

FIG. 11. Left – distribution of muons according to the distance to the surface that they have travelled through, right – distribution of the number of muons as a function of zenith and azimuth angles.

energy spectrum for a particular zenith and azimuthal angles, sampled in its turn from the angular distribution obtained using the MUSIC code. The size of the box (the probability of a muon to cross a particular surface of the box) is taken into account when generating muons. All energy spectra and angular distributions are stored on disk and read during the initialization at the beginning of each simulation run. The generator is fully integrated into `larsim` (within the LArSoft built upon *art* framework) since `v04_24_00`. The module is located at `larsim/larsim/EventGenerator/MuonPropagation/MUSUN_module.cc`. The configuration fcl file is in the same directory and is called `MUSUN.fcl`. MUSUN is ran with the fcl file `prodMUSUN_dune10kt.fcl`.

The muon rate through the surface of this box is 0.1579 Hz. This rate is used later

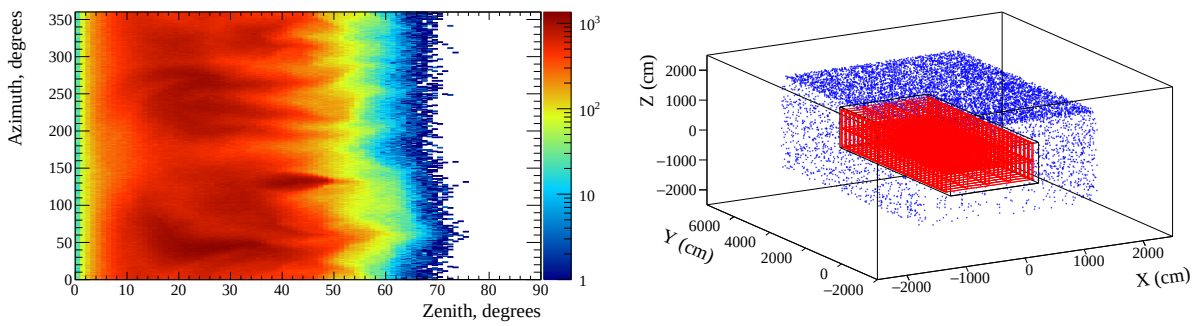

FIG. 12. Left – Colour plot of the number of muons as a function of zenith and azimuthal angles, right – muon positions as sampled on the surface of the box around the cavern with the cryostat.

to normalise the muon-induced background event rate in DUNE. (Note that the overall uncertainty in the muon flux is about 20%, see above.) The rate of muons passing through the active volume of liquid argon is 0.053 Hz so about 30% of muons generated on the surface of the box are passing through active argon (in fact having the track length of more than 1 m in the active volume.

Figures 10, 11 and 12 show various distributions of muons obtained with the MUSUN generator as incorporated into `larsim`.

B. Muon background for proton decay

There are a large number of proton decay modes where the sensitivity of DUNE may be comparable to or even exceeding that of Super-K/Hyper-K. The mode which is usually considered to be the 'golden' mode for the discovery at DUNE is: $p \to K^+\bar{\nu}$. This mode is dominant in most supersymmetric GUTs, many of which also favor other modes involving kaons in the final state. The decay modes with a charged kaon are unique for LAr experiments; since stopping kaons have a higher ionization density than pions or muons with the same momentum, a LArTPC could detect them with extremely high efficiency. In addition, many final states of K^+ decay would be fully reconstructable in a LArTPC.

The key signature for $p \to K^+\bar{\nu}$ is the presence of an isolated charged kaon (which would also be monochromatic for the case of free protons, with the momentum $p \approx 340$ MeV). The kaon emerges intact from the nucleus with 97% probability. The kaon momentum is smeared by the proton's Fermi motion and shifted downward by re-scattering [41]. The

kaon emerging from this process is below Cherenkov threshold in water, therefore a water Cherenkov detector would need to detect it after it stops, via its decay products. In LArTPC detectors, the K^+ can be tracked and identified via detailed analysis of its energy loss profile, and its kinetic energy measured by range. Additionally, all decay modes can be cleanly reconstructed and identified, including those with neutrinos, since the decaying proton is essentially at rest. With this level of detail, it is possible for a single event with an isolated kaon of the right momentum originating from a point within the fiducial volume, to provide overwhelming evidence for an observation of a proton decay.

The background for a proton decay search comes from atmospheric muons and neutrinos. If a muon passes through the detector, then the event can easily be reconstructed as a background muon-induced event and rejected. The current design of DUNE far detector suggests that the rate of muons passing through active LAr of a single module is about 0.05 Hz. With a full duration of event, limited by the maximum drift time of a few ms, rejecting all events with muons crossing the active volume of the TPC will result in less than 0.1% of dead time. Thus, only events with muons not crossing the active LAr volume may contribute to the background. Among these events the main danger comes from neutral kaons produced outside the TPC and undergoing inelastic scattering (primarily charge exchange) inside the TPC resulting in a single positive kaon detected. Figure 13 shows a schematic for such background event.

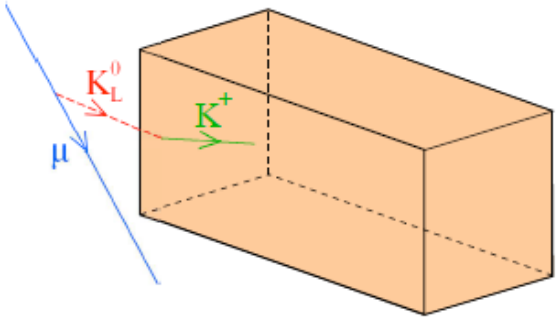

FIG. 13. A schematic showing a potential background events with a muon evading the detector but producing a neutral kaon that produces a positive kaon in its turn via charge exchange reaction. Positive kaon decay products are not shown. Taken from [38].

We have carried out initial simulations of muon-induced background in one DUNE module

with a fiducial mass of about 10.4 kt. By now (5 August 2016) 4×10^8 muons have been simulated and events in the detector analysed, corresponding to 80.32 years of live time of running one DUNE module. Only 'truth' parameters have been processed due to CPU time limitations and the full reconstruction chain not being fully ready for reconstructing large cosmic-ray events. The following cuts have been applied to reject muon-induced events: (i) no muon is in the detector active volume (the track length of the initial muon is less than 20 cm), (ii) the K^+ is fully contained within the fiducial volume ($>$ 2 cm from any TPC wall, similarly no energy deposition with 2 cm from the walls), (iii) the energy deposition from the K^+ and its descendants (excluding decay products) is $<$ 250 MeV (this includes smearing of the energy deposition due to energy resolution and nuclear effects in proton decay), (iv) the total energy deposition from the K^+, its descendants and decay products is $<$ 1 GeV, (v) energy deposition from other particles in the muon-induced cascade (i.e. excluding the energy deposition from the positive kaon, its descendants and decay products) is $<$ 30 MeV (otherwise this additional energy deposition can be clearly identified as such and the event be rejected as a background).

Figure 14 (left) shows the spectra of energy depositions from positive kaons after various cuts are applied. The three events shown by a dashed blue histogram are rejected after an additional cut on the energy deposition from other particles is applied. Figure 14 (right) shows the scatter plot of the kaon energy deposition vs that of other particles (excluding kaon and its decay products) for background events. For a proton decay event the energy deposition of other particles (x-axis on this plot) should be 0 but we have allowed for some hits to be missed or attributed to radiogenic background, hence imposed an upper limit of 50 keV on this energy deposition. The 3 events shown as red circles on the right plot (also shown as dashed blue histogram on the left plot) are rejected because the energy deposition from other particles exceeds 30 MeV. A few events inside the region of interest are rejected because of the energy deposition from within 2 cm of the walls (particles are entering the active volume from outside). Note that rejecting some of these events require a good timing resolution (light detection) to identify the correct start of the event. As a result of the analysis no event survived all the above cuts, resulting in an upper limit (at 90% CL) on the muon-induced background rate of 0.0029 events/kt/year.

Figure 15 shows the distribution of simulated events from proton decay mode $p \to K^+\bar{\nu}$. The x-axis shows the energy deposition from kaon decay products whereas the y-axis shows

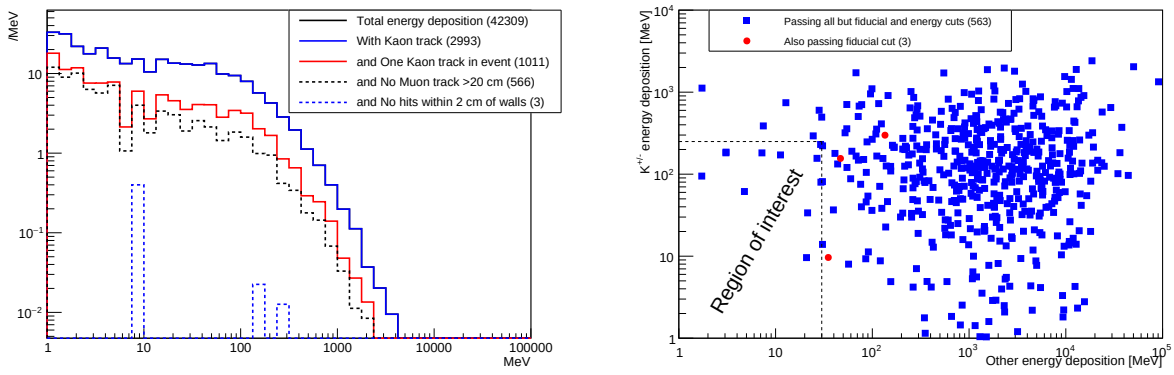

FIG. 14. Left – spectra of energy depositions from kaons after various cuts, right – scatter plot of a kaon energy deposition vs energy deposition of other particles (excluding kaon and its decay products) for background events.

the energy deposition from the positive kaon. Almost all kaons deposit less than 250 MeV inside the active volume which justifies the choice of cuts for background events. Note that the energy deposition from other particles (excluding kaons and the products of their interactions and decays) should be zero for this mode of proton decay which serves as a good selection criterium to reject background events (currently required to be less than 30 MeV but can be tuned further).

C. Cosmic-ray event reconstruction

Reconstruction in LArTPCs is a complex process requiring numerous steps from hit reconstruction to hit disambiguation, clustering and ultimately combining clusters into tracks. As the process has multiple steps there are a suite of options at each stage, for this study though the following modules have been used:

- Gaussian hit finder,
- Disambiguation algorithm tuned for the far detector,
- Line cluster, clustering algorithm,
- Projection matching tracking algorithm (PMTrack).

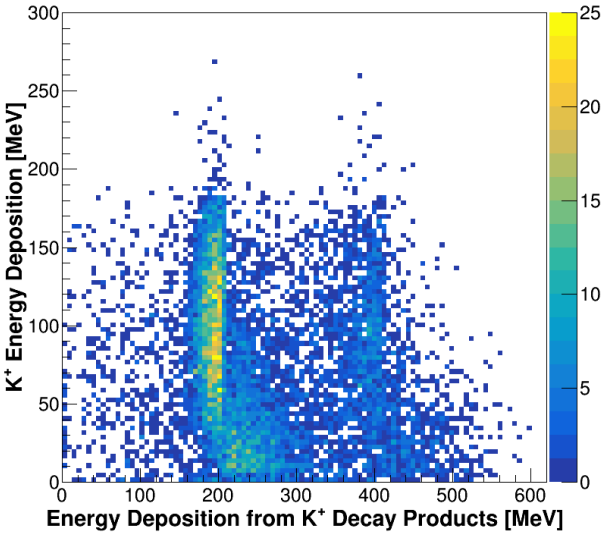

FIG. 15. Distribution of simulated events from proton decay mode $p \to K^+\bar{\nu}$. The x-axis shows the energy deposition from kaon decay products whereas the y-axis shows the energy deposition from the positive kaon.

Many of the reconstruction algorithms were tuned and developed for significantly smaller detectors than the far detector such as the 35 ton prototype. This means that tuning of the algorithms is required to achieve a high reconstruction efficiency. This tuning was achieved through a detailed study of 100 simulated muons using the MUSUN generator discussed above. Properties of the reconstruction to be improved were identified and the tuning required to do so is illustrated below.

Two views are shown for each event, one called 'Ortho3D' which has two dimensional representations of the detector in the XZ and YZ planes. Within each plane the TPCs are shown as regions contained within grey dashed lines. The reconstructed tracks are shown as bold coloured lines, and are labelled with their reconstructed track number which increases from 0. The second view is that of the wire planes for a given TPC. The TPC number is shown on the left hand side of the image. Three wire planes are visible, which in descending order are the collection plane, the U induction plane and the V induction plane. The plot for each plane shows the wire number on the plane (increasing from 0) against TPC tick (in units of 500 ns). The charge deposited on a wire at a given time is shown using a colour

scale shown on the right of each plane. At the bottom of the image is a plot showing the charge deposited on a given wire for a range of times, the blue line shows the de-convoluted signal and the orange lines displays the reconstructed hits.

Many through-going muons were originally reconstructed as multiple tracks as opposed to a single track. These track separations regularly occurred as a muon crossed a TPC boundary, where there is an ∼5 cm area of un-instrumented LAr. This meant that the track sections were not merged into a single track. Upon allowing for tracks to be merged with larger separations many of the un-merged tracks are observed to be successfully merged. An example of a merged through-going muon is shown in Figure 16.

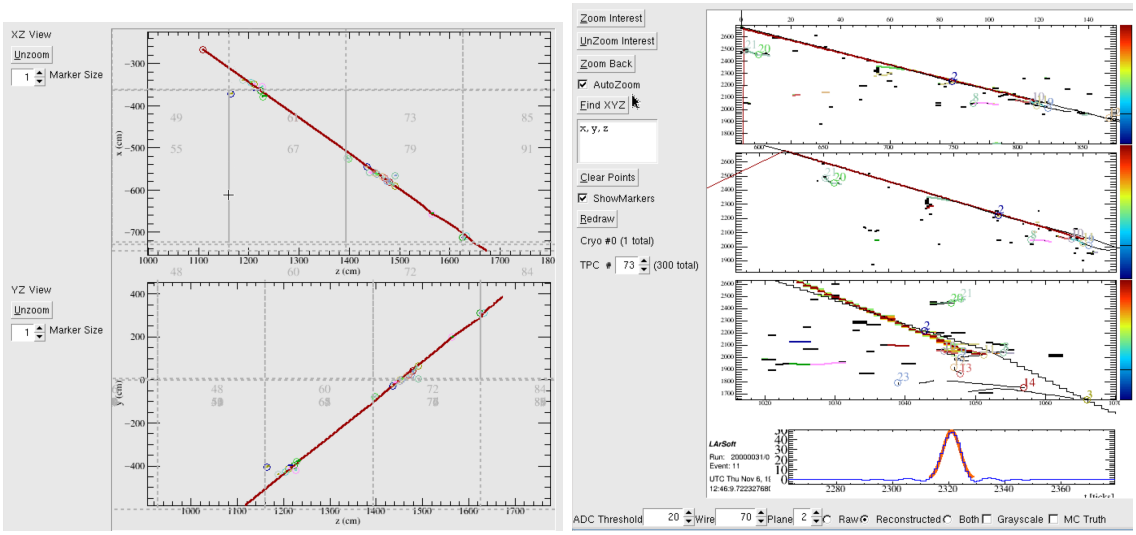

FIG. 16. An example of a well reconstructed through going muon track. Left image shows the Ortho3D view, right image shows the LArSoft wire plane display.

Another reason for split tracks is due to high energy delta-rays. These large energy depositions create additional large clusters to be reconstructed around the main track causing the track to be split. Further study is required to mitigate the effect of high-energy delta-rays, an example of which is shown in Figure 17.

High-energy muons can produce large showers. These large energy depositions cause many short ($\leq$10 cm) tracks to be reconstructed. The effect of this is that the reconstruction appears to perform badly due to a large excess of reconstructed tracks at short track

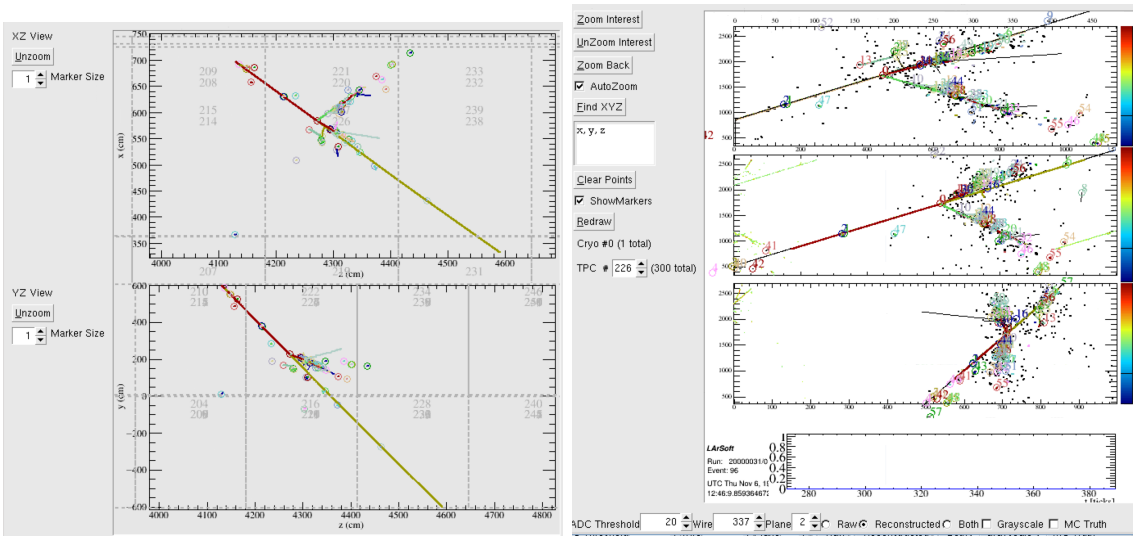

FIG. 17. An example of a delta-ray causing a through-going muon to be split into two tracks. Left image shows the Ortho3D view, right image shows the wire plane display.

lengths, however the through-going muon track is often fully reconstructed. An example of a high-energy shower is shown in Figure 18.

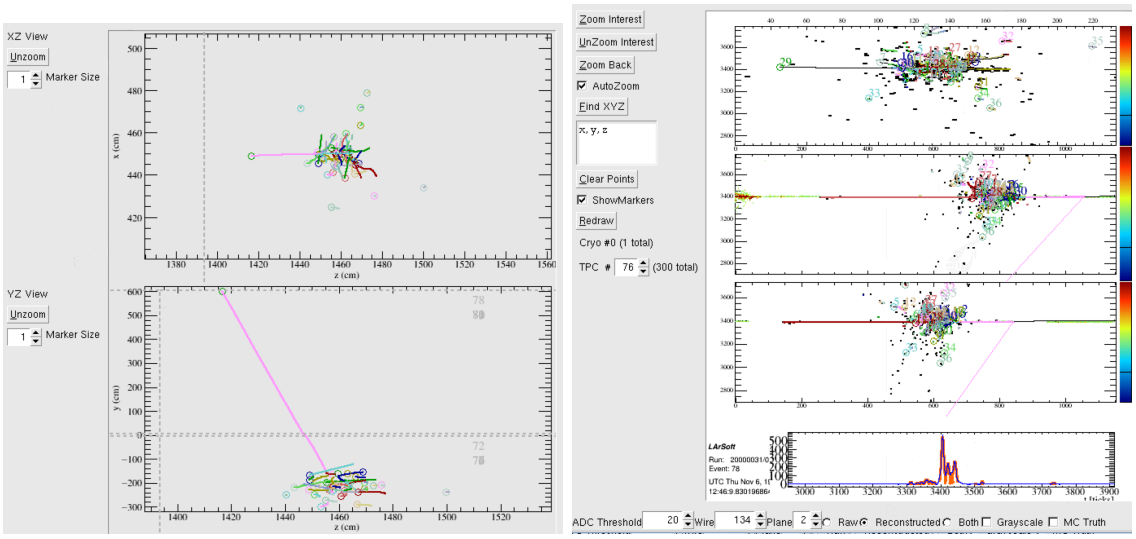

FIG. 18. An example of a high-energy shower in the detector around a through going muon. Left image shows the Ortho3D view, right image shows the wire plane display.

Occasionally hits within TPCs can be successfully reconstructed into clusters which are not merged to produce tracks. It was observed that this is due to one or more of the clusters

being incorrectly identified as a delta-ray causing the track to be reconstructed outside the TPC and being discarded. The effect of this was greatly reduced by allowing for a greater variation in TPC containment, however occasional examples can still be found. An example of an un-merged track is shown in Figure 19.

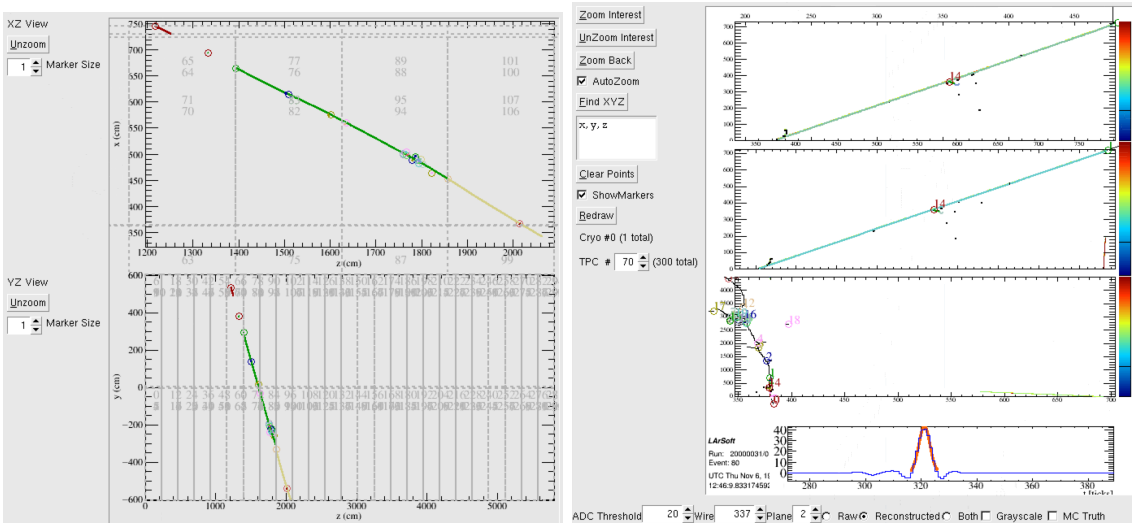

FIG. 19. An example of an event where the merger of clusters has failed causing sections of track to be dropped. Left image shows the Ortho3D view, right image shows the wire plane display.

Reconstruction of kaons of the energy which would be observed in proton decay are being studied by the reconstruction working group and is not considered in here.

V. ACKNOWLEDGMENTS

The global detector positioning and orientation used in the MUSUN code was provided by the staff of the SURF facility (many thanks to J. Willhite, J. Heise, T. Lundin and others). The surface profile has been converted into the slant depth distribution for MUSIC by Martin Richardson (Sheffield). The original conversion of the MUSIC from FORTRAN to C++ for the LZ experiment at SURF has been done by Kareem Kazkaz (LLNL) and David Woodward (Sheffield). We acknowledge the support from, and very useful discussions with the Simulation and Reconstruction working group (Tom Junk, Tingjun Yang, Dorota Stefan,

Robert Sulej and others).

---

[1] R. Acciarri et al. (DUNE) (2015), 1512.06148.

[2] A. Bueno, Z. Dai, Y. Ge, M. Laffranchi, A. J. Melgarejo, A. Meregaglia, S. Navas, and A. Rubbia, JHEP **04**, 041 (2007), hep-ph/0701101.

[3] C. Andreopoulos et al., Nucl. Instrum. Meth. **A614**, 87 (2010), 0905.2517.

[4] C. Andreopoulos, C. Barry, S. Dytman, H. Gallagher, T. Golan, R. Hatcher, G. Perdue, and J. Yarba (2015), 1510.05494.

[5] K. A. Olive et al. (Particle Data Group), Chin. Phys. **C38**, 090001 (2014).

[6] M. Sorel, Expanding GENIE's Nucleon Decay Tools, https://indico.fnal.gov/getFile.py/access?contribId=4&resId=0&materialId=slides&confId=12549.

[7] T. Yang, Simulation of Nucleon Decays, https://indico.fnal.gov/getFile.py/access?contribId=5&resId=0&materialId=slides&confId=12549.

[8] G. Santucci, Far detector simulation and reconstruction chain for non-beam events, https://indico.fnal.gov/getFile.py/access?contribId=59&sessionId=19&resId=0&materialId=slides&confId=10612.

[9] A. Ferrari, P. R. Sala, A. Fasso, and J. Ranft (2005).

[10] K. Wood, Vertex Assignment Correction in NDK Generation, https://indico.fnal.gov/getFile.py/access?contribId=5&resId=0&materialId=slides&confId=12377.

[11] J. Hewes, Neutron-antineutron oscillation in DUNE", https://indico.fnal.gov/getFile.py/access?contribId=58&sessionId=31&resId=0&materialId=slides&confId=10276.

[12] H. Mendez and N. Martinez, First look at fully reconstructed $p \to l^+\rho^0$ and $p \to \mu^+K^0$ events, https://indico.fnal.gov/getFile.py/access?contribId=3&resId=0&materialId=slides&confId=12549.

[13] A. Higuera, Proton decay, $p \to \bar{\nu}K^+$, https://indico.fnal.gov/getFile.py/access?contribId=2&resId=0&materialId=slides&confId=12651.

[14] M. Antonello et al., Adv. High Energy Phys. **2013**, 260820 (2013), 1210.5089.

[15] A. Higuera, Far detector tracking efficiencies, https://indico.fnal.gov/getFile.py/access?contribId=63&sessionId=19&resId=0&materialId=slides&confId=10612.

[16] R. Acciarri et al. (ArgoNeuT), JINST **8**, P08005 (2013), 1306.1712.

[17] K. Wood, Flash Finding Efficiencies for PDK events, https://indico.fnal.gov/getFile.py/access?contribId=0&resId=0&materialId=slides&confId=12651.

[18] M. Goodman and L. Lin, Comprehensive list of nucleon decay modes (DUNE-doc-679), http://docs.dunescience.org:8080/cgi-bin/ShowDocument?docid=679.

[19] M. Sorel, ndksens, A tool for evaluating NDK sensitivities, https://indico.fnal.gov/getFile.py/access?contribId=57&sessionId=31&resId=0&materialId=slides&confId=10276.

[20] G. D. Barr, T. K. Gaisser, P. Lipari, S. Robbins, and T. Stanev, Phys. Rev. **D70**, 023006 (2004), astro-ph/0403630.

[21] G. Battistoni, A. Ferrari, P. Lipari, T. Montaruli, P. R. Sala, and T. Rancati, Astropart. Phys. **12**, 315 (2000), hep-ph/9907408.

[22] M. Sajjad Athar, M. Honda, T. Kajita, K. Kasahara, and S. Midorikawa, Phys. Lett. **B718**, 1375 (2013), 1210.5154.

[23] J. Losecco, Honda atmospheric flux calculation for Homestake, https://indico.fnal.gov/materialDisplay.py?contribId=3&materialId=slides&confId=11533.

[24] M. Rafi Alam, I. Ruiz Simo, M. Sajjad Athar, and M. J. Vicente Vacas, Phys. Rev. **D82**, 033001 (2010), 1004.5484.

[25] M. Alam et al. (2015), 1512.06882.

[26] A. Ioannisian, Exploring the Earth with neutrinos, https://indico.fnal.gov/materialDisplay.py?contribId=0&materialId=slides&confId=10573.

[27] L. Fantini and G. VanWinkle, Measuring the azimuthal angle distribution of atmospheric neutrinos in DUNE, https://indico.fnal.gov/materialDisplay.py?contribId=3&materialId=slides&confId=12005.

[28] E. Richard et al. (Super-Kamiokande) (2015), 1510.08127.

[29] H. Gallagher, Atmospheric event generators, https://indico.fnal.gov/materialDisplay.py?contribId=2&materialId=slides&confId=12274.

[30] V. A. Kudryavtsev, Comput. Phys. Commun. **180**, 339 (2009), 0810.4635.

[31] V. A. Kudryavtsev, N. J. C. Spooner, and J. E. McMillan, Nucl. Instrum. Meth. **A505**, 688 (2003), hep-ex/0303007.

[32] P. Antonioli, C. Ghetti, E. V. Korolkova, V. A. Kudryavtsev, and G. Sartorelli, Astropart. Phys. **7**, 357 (1997), hep-ph/9705408.

[33] V. A. Kudryavtsev, E. V. Korolkova, and N. J. C. Spooner, Phys. Lett. **B471**, 251 (1999), hep-ph/9911493.

[34] D. M. Mei, C. Zhang, K. Thomas, and F. Gray, Astropart. Phys. **34**, 33 (2010), 0912.0211.

[35] C. Zhao (USD), private communication.

[36] F. E. Gray, C. Ruybal, J. Totushek, D. M. Mei, K. Thomas, and C. Zhang, Nucl. Instrum. Meth. **A638**, 63 (2011), 1007.1921.

[37] J. Heise, AIP Conf. Proc. **1604**, 331 (2014), 1401.0861.

[38] M. Richardson, Ph.D. thesis, University of Sheffield (2016).

[39] M. L. Cherry, M. Deakyne, K. Lande, C. K. Lee, R. I. Steinberg, B. T. Cleveland, and E. J. Fenyves, Phys. Rev. **D27**, 1444 (1983).

[40] N. Abgrall et al. (Majorana) (2016), 1602.07742.

[41] D. Stefan and A. M. Ankowski, Acta Phys. Polon. **B40**, 671 (2009), 0811.1892.